Modeling the Fabrication of Hollow Fibers: Capillary Drawing

Alistair D. Fitt, Kentaro Furusawa, Tanya M. Monro, and Colin P. Please

***Abstract*—A method for modeling the fabrication of small-scale hollow glass capillaries is developed. The model is based on an asymptotic analysis of the Navier-Stokes equations, which yields a simple closed-form solution for this problem. We demonstrate the validity of this approach using experimental data and use it to make predictions for a range of regimes of interest for the development of microstructured optical fiber technology.**

***Index Terms*—Mathematical modeling, optical fiber, optical fiber applications, optical fiber fabrication, optical fiber theory.**

I. Introduction

THE past few years have seen the emergence of an important new class of optical fiber, the holey or microstructured fiber. The transverse profile of a microstructured fiber contains an array of air holes that run along the fiber length. Holey or microstructured fibers guide light due to the effective refractive index difference between the solid core and the cladding, which is laced with air holes. These fibers may be made from a single material, often pure silica; two examples are shown in Fig. 1. The effective index contrast can be a strong function of wavelength of the light guided by the fiber. This is particularly striking when the structure scale is small, and leads to a host of highly unusual and tailorable optical properties [1]–[4]. For example, holey fibers with small holes can be endlessly single-mode, regardless of the wavelength [1]. Depending on the cladding configuration, such fibers can have mode-area values ranging over three orders of magnitude, and can display anomalous dispersion throughout the visible spectrum.

The presence of air holes in such microstructured fibers opens up a vast new range of potential applications. These range from small mode area, highly nonlinear fibers for novel nonlinear devices [4] to large mode area fibers for high-power delivery [5], [3]. Different cladding structures may also allow dispersion compensation [6] or dispersion flattening for wavelength division multiplexing (WDM) telecommunications systems [7], [8]. In addition, the presence of air holes may be directly exploited for applications in evanescent-field sensing [2].

Another type of microstructured optical fiber is the photonic-bandgap fiber. These fibers guide light by making use of the photonic bandgaps that can occur in a periodic structure [9]. A further example of a microstructured fiber is the atom-guiding fiber [10]. In this latter example, metal electrodes are inserted into four holes in the fiber, and by running currents along these wires, a magnetic potential can be established that then acts to guide atoms down another hole in the center of the fiber.

Microstructured fibers are produced by drawing a macroscopic preform (typically a few centimeters in diameter) down into a fiber (typically 125 μm in diameter) using a conventional fiber-drawing tower. These preforms can be made in a variety of ways, and the two most common approaches are described briefly here. One method involves stacking small capillaries around a solid rod, which ultimately forms the fiber core. This approach is generally preferred when large air holes are required in the final fiber structure. Alternatively, the required arrangement of holes can be drilled directly in a solid glass blank. This works well when only a few well-separated holes are required, as, for example, in the case of atom-guiding fibers.

Regardless of the method used to produced the preform, the geometry of the final fiber can be modified significantly by controlling the parameters used in the drawing process, i.e., the temperature of the furnace, the speed at which the preform is fed into this furnace, and the draw speed. For example, when high temperatures or low draw speeds are used, the air holes in the cladding reduce in size and may even close completely because of surface-tension effects. It is often desirable to take advantage of this collapse process to tune the final size of the small air holes in the resulting structure during fabrication. In this way, a range of fibers with dramatically different optical properties can be produced from a single preform. At the other extreme, large holes are required to obtain tight mode confinement or full photonic bandgaps, and so it is desirable to avoid any collapse of the air holes.

Theoretical predictive studies of fiber drawing grew, for the most part, out of theory that had already been developed for the textile industry to model the spinning of molten threadlines [11]–[14]. This general methodology was then adapted to optical fiber drawing. A great deal of the literature concerns fiber-drawing models that are essentially small perturbations about prescribed steady unidirectional extensional flows. Various studies have considered the additional effects of heat transfer [15], surface tension [16], weak unsteadiness [12], and inertia [13]. The effects of both gravity and inertia were included in a general theory of slender viscous fibers of arbitrary cross section [17]. Fiber breaking has also been considered. In [18], Dewynne *et al.* proposed an asymptotic model of fiber drawing that was essentially similar to [16], but showed that, unless the initial conditions possess certain singularities, the cross-sectional area cannot be made to vanish in finite time.

Manuscript received May 22, 2001; revised August 9, 2001. This work was supported in part by a Royal Society University Research Fellowship.

A. D. Fitt and C. P. Please are with the Faculty of Mathematical Studies, University of Southampton, Southampton SO17 1BJ, U.K. (e-mail: adf@maths.soton.ac.uk; cpp@maths.soton.ac.uk).

K. Furusawa and T. M. Monro are with the Optoelectronics Research Centre, University of Southampton, Southampton SO17 1BJ, U.K. (e-mail: kf@orc.soton.ac.uk; tmm@orc.soton.ac.uk).

Publisher Item Identifier S 0733-8724(01)10198-2.

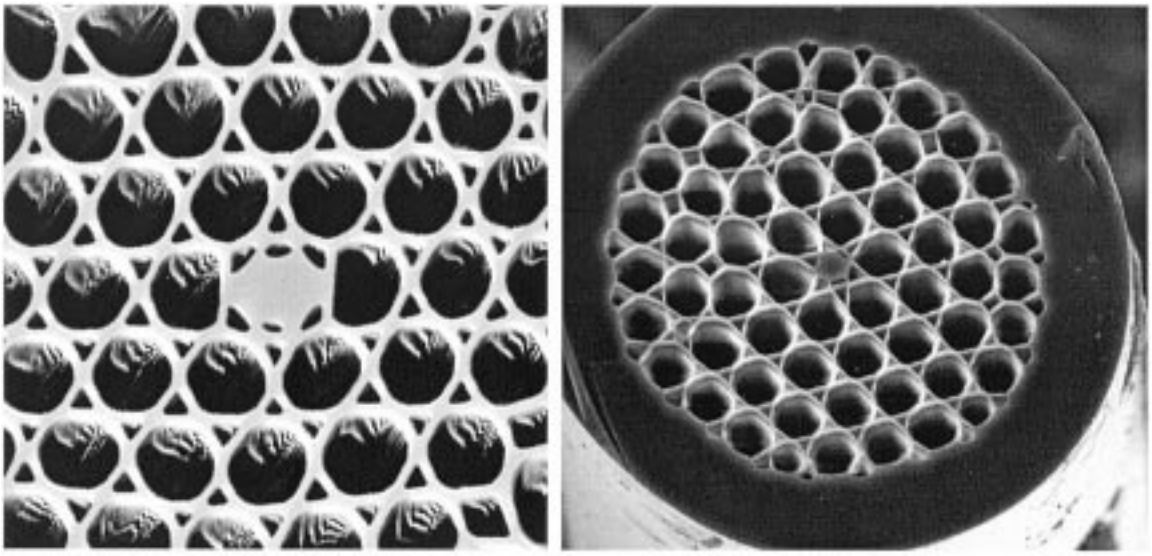

(a) (b)

Fig. 1. Two typical silica holey fibers. The fibers on the left and right have core diameters of approximately 2.5 μm and 5 μm, respectively.

A number of purely numerical studies of optical-fiber drawing have also been made (see, for example [19], [20], and [21]). It does not appear, however, that any detailed theory has yet been proposed for fibers that have a cross section containing holes. The drawing of thin-walled viscous capillaries was modeled in [22] and [23] (see also [24]), and [25] made some basic estimates of the strength of hollow glass fibers for use in reinforced plastics. Because the optical properties of a microstructured fiber depend critically upon the sizes and locations of the holes in the cladding, it is important to be able to predict how the fabrication parameters influence the final fiber cross section. In order to accomplish this, we develop below a theoretical framework for investigating the drawing of glass capillaries. Our analysis exploits the long thin geometry of the draw region and may be applied to capillaries of arbitrary dimensions. The fabrication of capillaries is an important element of the manufacture of microstructured fibers, and, hence, the established theoretical framework forms the foundation for modeling the fabrication of more complex structures.

II. Mathematical Modeling

To develop a mathematical model for the process of capillary drawing that is capable of including effects such as surface tension, varying viscosity, and internal hole overpressure, we begin from the incompressible Navier–Stokes equations (see, for example [21])

$$\rho(u_t + uu_x + wu_r) = -p_x + \frac{1}{r}(\mu r u_r)_r + (2\mu u_x)_x + \frac{1}{r}(\mu r w_x)_r + \rho g \quad (1)$$

$$\rho(w_t + uw_x + ww_r) = -p_r + \mu\left(\frac{1}{r}(rw)_r\right)_r + (\mu w_x)_x + \mu_x u_r + 2\mu_r w_r \quad (2)$$

$$u_x + \frac{1}{r}(rw)_r = 0. \quad (3)$$

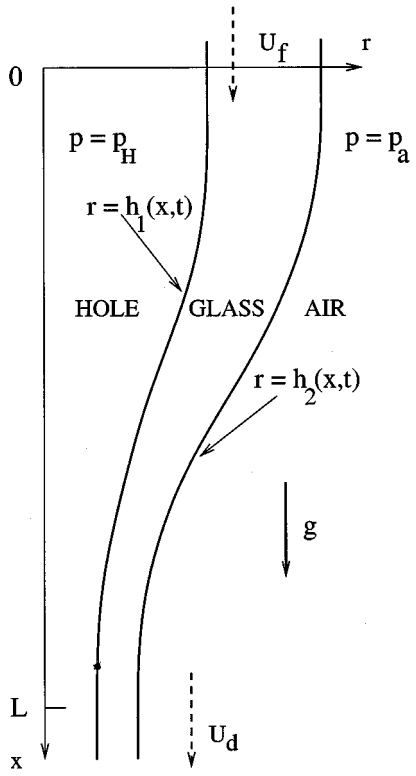

Fig. 2. Schematic diagram and nomenclature for capillary.

In (1)–(3), derivatives are denoted by subscripts, x measures the distance along the axis of a capillary, and r measures the distance normal to it. The flow and the geometry have been assumed to be axisymmetric, and are, therefore, independent of the azimuthal angle θ. The velocity $\boldsymbol{q}$ of the molten glass is denoted by $\boldsymbol{q} = u\boldsymbol{e}_x + w\boldsymbol{e}_r$ where $\boldsymbol{e}_x$ and $\boldsymbol{e}_r$ are unit vectors in the x and r directions, respectively. A schematic diagram of the geometry of the capillary is shown in Fig. 2.

The density of the glass is denoted by ρ. Because glass density is known to be only weakly dependent on temperature, incom-

pressibility has been assumed and we have used the density of solidified glass throughout. Pressure is denoted by p, g is the acceleration due to gravity, and dynamic viscosity and surface tension are denoted by μ and γ, respectively. For simplicity, we assume that the furnace temperature T is known, although it may depend upon x, and that the thinness of the fiber means that the temperature (and, thus, the viscosity) is uniform over the cross section of a capillary. If this is not the case, then the analysis may be extended to take into account temperature variations in a fairly obvious way; we do not pursue this further here. We also neglect the temperature variation of both ρ and γ, because this is, typically, a very weak effect (see, for example, [26]).

We now assume that the inner and outer radii of the capillary are denoted by $r = h_1(x,t)$ and $r = h_2(x,t)$, respectively. Thus, (1)–(3) apply in the region $h_1 \le r \le h_2$ and must be solved subject to suitable boundary and initial conditions, which will be considered presently.

A. Asymptotic Analysis

It is now appropriate to nondimensionalize (1)–(3) to take advantage of the small parameters that are present in the problem. On setting $x = L\bar{x}, r = h\bar{r}, t = (L/U)\bar{t}$, $u = U\bar{u}, w = (Uh/L)\bar{w}, h_1 = h\bar{h}_1$, $h_2 = h\bar{h}_2, \mu = \mu_0\bar{\mu}$, and $p = (\mu_0 UL/h^2)\bar{p}$, where an overbar denotes a nondimensional quantity and L denotes a typical draw length (i.e., the distance over which the preform is heated by the furnace), h denotes a typical drawn capillary size, U denotes a typical draw speed, and μ_0 denotes a typical glass viscosity, the equations become

$$\epsilon^2 \mathrm{Re}[\bar{u}_{\bar{t}} + \bar{u}\bar{u}_{\bar{x}} + \bar{w}\bar{u}_{\bar{r}}] = -\bar{p}_{\bar{x}} + \epsilon^2(2\bar{\mu}\bar{u}_{\bar{x}})_{\bar{x}} + \frac{1}{\bar{r}}(\bar{\mu}\bar{r}\bar{u}_{\bar{r}})_{\bar{r}} + \frac{\epsilon^2}{\bar{r}}(\bar{\mu}\bar{r}\bar{w}_{\bar{x}})_{\bar{r}} + \frac{\epsilon^2 \mathrm{Re}}{Fr}$$

$$\epsilon^2 \mathrm{Re}[\bar{w}_{\bar{t}} + \bar{u}\bar{w}_{\bar{x}} + \bar{w}\bar{w}_{\bar{r}}] = -\frac{\bar{p}_{\bar{r}}}{\epsilon^2} + \epsilon^2(\bar{\mu}\bar{w}_{\bar{x}})_{\bar{x}} + \bar{\mu}\left(\frac{1}{\bar{r}}(\bar{r}\bar{w})_{\bar{r}}\right)_{\bar{r}} + \bar{\mu}_{\bar{x}}\bar{u}_{\bar{r}} + 2\bar{\mu}_{\bar{r}}\bar{w}_{\bar{r}}$$

$$\bar{u}_{\bar{x}} + \frac{1}{\bar{r}}(\bar{r}\bar{w})_{\bar{r}} = 0$$

where the nondimensional parameters ϵ and the Reynolds and Froude numbers are given respectively by

$$\epsilon = \frac{h}{L} \qquad \mathrm{Re} = \frac{LU\rho}{\mu_0} \qquad Fr = \frac{U^2}{gL}.$$

For the particular parameter regimes of interest in this study, the drawing length L is 3 cm, and a typical drawn capillary has an outside diameter (OD) of 1 mm. Thus, $\epsilon \sim 1/30$, and we therefore treat ϵ as a small parameter. We retain the gravity and inertia terms in the equations because they may be important in specific regions of the flow, and their retention leaves the analysis essentially unchanged. The leading-order equations in ϵ are now satisfied by the obvious *ansatz*

$$\bar{u} = \bar{u}_0(\bar{x},\bar{t}) + \epsilon^2\bar{u}_1(\bar{x},\bar{r},\bar{t}) + \cdots$$
$$\bar{w} = \bar{w}_0(\bar{x},\bar{r},\bar{t}) + \epsilon^2\bar{w}_1(\bar{x},\bar{r},\bar{t}) + \cdots$$
$$\bar{p} = \bar{p}_a + \epsilon^2\bar{P}(\bar{x},\bar{r},\bar{t}) + \cdots$$

where $\bar{p}_a$ denotes the nondimensional ambient pressure, defined by $p_a = (\mu_0 UL/h^2)\bar{p}_a$, and from (3) we have

$$\bar{w}_0 = -\frac{\bar{r}\bar{u}_{0\bar{x}}}{2} + \frac{\bar{A}}{\bar{r}}$$

where the function $\bar{A}(\bar{x},\bar{t})$ is to be determined. To order ϵ^2, the $\bar{x}$-momentum equation is now

$$\mathrm{Re}(\bar{u}_{0\bar{t}} + \bar{u}_0\bar{u}_{0\bar{x}}) + \bar{P}_{\bar{x}} - \frac{\mathrm{Re}}{Fr} - 2(\bar{\mu}\bar{u}_{0\bar{x}})_{\bar{x}} + \bar{\mu}\bar{u}_{0\bar{r}\bar{r}} = \frac{1}{\bar{r}}(\bar{\mu}\bar{r}\bar{u}_{1\bar{r}})_{\bar{r}} \quad (4)$$

and the $\bar{r}$-momentum equation gives

$$0 = -\bar{P}_{\bar{r}} + \bar{\mu}\left(\frac{1}{\bar{r}}(\bar{r}\bar{w}_0)_{\bar{r}}\right)_{\bar{r}}$$

which yields $\bar{P}_{\bar{r}} = 0$, so that $\bar{P}$ is a function of $\bar{x}$ and $\bar{t}$ alone.

To close the problem, initial conditions must be given for each of the unknowns and we must specify kinematic, normal, and tangential stress conditions on the two free boundaries. The kinematic conditions amount simply to the fact that the total derivative of each boundary is zero at that boundary. Thus, $D(r - h_i(x,t))/Dt = (\partial_t + (\boldsymbol{q}\cdot\nabla))(r - h_i(x,t)) = 0$ on $r = h_i(x,t)$ $(i = 1,2)$, and, so, in nondimensional form, we find that

$$\bar{w}_0 = \bar{h}_{1\bar{t}} + \bar{u}_0\bar{h}_{1\bar{x}}, \quad \text{at } \bar{r} = \bar{h}_1 \quad (5)$$
$$\bar{w}_0 = \bar{h}_{2\bar{t}} + \bar{u}_0\bar{h}_{2\bar{x}}, \quad \text{at } \bar{r} = \bar{h}_2. \quad (6)$$

In practice, it is possible to influence the manufacture of capillaries or optical fibers that contain holes by pressurizing the holes. Therefore, we wish to include this possibility in our modeling. The normal stress boundary conditions must, thus, include both the surface tension coefficient γ and the fiber hole pressure p_H. Defining the nondimensional fiber hole pressure by $p_H = (\mu_0 UL/h^2)\bar{p}_H$, we see immediately that we must further write

$$\bar{p}_H = \bar{p}_a + \epsilon^2\bar{p}_o$$

where $\bar{p}_o$ is the nondimensional hole overpressure. This scaling reflects the fact that, unless the fiber hole pressure is within $O(\epsilon^2)$ of the ambient pressure, the capillary will either collapse immediately or explode.

The normal stress boundary conditions may now be applied. The nondimensional stress tensor $\bar{\mathcal{T}}$ is given by

$$\bar{\mathcal{T}} = \frac{\mu_0 U}{L}\begin{pmatrix} -\bar{p}/\epsilon^2 + 2\bar{\mu}\bar{u}_{\bar{x}} & \bar{\mu}\bar{u}_{\bar{r}}/\epsilon + \epsilon\bar{\mu}\bar{w}_{\bar{x}} \\ \bar{\mu}\bar{u}_{\bar{r}}/\epsilon + \epsilon\bar{\mu}\bar{w}_{\bar{x}} & -\bar{p}/\epsilon^2 + 2\bar{\mu}\bar{w}_{\bar{r}} \end{pmatrix}.$$

If we now denote the unit outward-pointing normal to $\bar{r} = \bar{h}_i$ $(i = 1,2)$ by $\hat{\boldsymbol{n}}_i$, the nondimensional normal stress conditions are

$$-\hat{\boldsymbol{n}}_1^T\bar{\mathcal{T}}\hat{\boldsymbol{n}}_1 + \frac{\bar{\gamma}\mu_0 U}{\bar{h}_1 L} = \frac{\bar{p}_h\mu_0 U}{L\epsilon^2}, \quad \text{at } \bar{r} = \bar{h}_1$$
$$-\hat{\boldsymbol{n}}_2^T\bar{\mathcal{T}}\hat{\boldsymbol{n}}_2 - \frac{\bar{\gamma}\mu_0 U}{\bar{h}_2 L} = \frac{\bar{p}_a\mu_0 U}{L\epsilon^2}, \quad \text{at } \bar{r} = \bar{h}_2$$

where a nondimensional surface tension coefficient has been defined by $\gamma = \mu_0 U\epsilon\bar{\gamma}$. We further assume that the tangential stress on both of the fiber boundaries is zero. Thus, for $i = 1,2$

$$\hat{\boldsymbol{t}}_i^T\bar{\mathcal{T}}\hat{\boldsymbol{n}}_i = 0$$

at $\bar{r} = \bar{h}_i$, where $\hat{\boldsymbol{t}}_i$ is the relevant unit tangent vector. The normal and tangential stress conditions may now be expanded according to the *ansatz* for $\bar{u}, \bar{w}$, and $\bar{p}$. With

$$\hat{\boldsymbol{n}}_i^T = \frac{(-1)^{i+1}}{\sqrt{1+\epsilon^2\bar{h}_{i\bar{x}}^2}}(\epsilon\bar{h}_{i\bar{x}}, -1) \qquad \hat{\boldsymbol{t}}_i^T = \frac{(-1)^{i+1}}{\sqrt{1+\epsilon^2\bar{h}_{i\bar{x}}^2}}(1, \epsilon\bar{h}_{i\bar{x}})$$

we find that

$$-\frac{\bar{\gamma}}{\bar{h}_1} - \bar{P} + 2\bar{\mu}\bar{w}_{0\bar{r}} + \bar{p}_o = 0, \quad \text{at } \bar{r} = \bar{h}_1$$
$$\frac{\bar{\gamma}}{\bar{h}_2} - \bar{P} + 2\bar{\mu}\bar{w}_{0\bar{r}} = 0, \quad \text{at } \bar{r} = \bar{h}_2$$
$$2\bar{h}_{1\bar{x}}(\bar{u}_{0\bar{x}} - \bar{w}_{0\bar{r}}) - \bar{w}_{0\bar{x}} = \bar{u}_{1\bar{r}}, \quad \text{at } \bar{r} = \bar{h}_1$$
$$2\bar{h}_{2\bar{x}}(\bar{u}_{0\bar{x}} - \bar{w}_{0\bar{r}}) - \bar{w}_{0\bar{x}} = \bar{u}_{1\bar{r}}, \quad \text{at } \bar{r} = \bar{h}_2.$$

A closed system of equations may now be derived. We integrate $\bar{r}$ times the x-momentum (4) from $\bar{r} = \bar{h}_1$ to $\bar{h}_2$ to yield

$$\frac{(\bar{h}_2^2 - \bar{h}_1^2)}{2}\left[\mathrm{Re}(\bar{u}_{0\bar{t}} + \bar{u}_0\bar{u}_{0\bar{x}}) + \bar{P}_{\bar{x}} - \frac{\mathrm{Re}}{Fr} - 2(\bar{\mu}\bar{u}_{0\bar{x}})_{\bar{x}} + \bar{\mu}\bar{u}_{0\bar{x}\bar{x}}\right] = (\bar{\mu}\bar{h}_2\bar{u}_{1\bar{r}})|_{\bar{h}_2} - (\bar{\mu}\bar{h}_1\bar{u}_{1\bar{r}})|_{\bar{h}_1}. \quad (7)$$

We may now evaluate the kinematic conditions (5) and (6) to yield

$$(\bar{h}_1^2)_{\bar{t}} + (\bar{h}_1^2\bar{u}_0)_{\bar{x}} = 2\bar{A} \quad (8)$$
$$(\bar{h}_2^2)_{\bar{t}} + (\bar{h}_2^2\bar{u}_0)_{\bar{x}} = 2\bar{A}. \quad (9)$$

The normal and tangential stress boundary conditions, which are to be applied at $\bar{r} = \bar{h}_1$ and $\bar{r} = \bar{h}_2$, give, respectively

$$0 = -\frac{\bar{\gamma}}{\bar{h}_1} - \bar{P} + \bar{p}_o + \bar{\mu}\left(-\bar{u}_{0\bar{x}} - \frac{2\bar{A}}{\bar{h}_1^2}\right) \quad (10)$$
$$0 = \frac{\bar{\gamma}}{\bar{h}_2} - \bar{P} + \bar{\mu}\left(-\bar{u}_{0\bar{x}} - \frac{2\bar{A}}{\bar{h}_2^2}\right) \quad (11)$$
$$\bar{u}_{1\bar{r}}|_{\bar{r}=\bar{h}_1} = 2\bar{h}_{1\bar{x}}\left(\frac{3\bar{u}_{0\bar{x}}}{2} + \frac{\bar{A}}{\bar{h}_1^2}\right) - \frac{\bar{A}_{\bar{x}}}{\bar{h}_1} + \frac{\bar{h}_1\bar{u}_{0\bar{x}\bar{x}}}{2} \quad (12)$$
$$\bar{u}_{1\bar{r}}|_{\bar{r}=\bar{h}_2} = 2\bar{h}_{2\bar{x}}\left(\frac{3\bar{u}_{0\bar{x}}}{2} + \frac{\bar{A}}{\bar{h}_2^2}\right) - \frac{\bar{A}_{\bar{x}}}{\bar{h}_2} + \frac{\bar{h}_2\bar{u}_{0\bar{x}\bar{x}}}{2}. \quad (13)$$

The system is now closed, as (7), (8), (9), and (10)–(13) comprise seven equations for the seven unknowns $\bar{h}_1, \bar{h}_2, \bar{A}, \bar{P}, \bar{u}_0, \bar{u}_{1r}|_{\bar{h}_1}$, and $\bar{u}_{1r}|_{\bar{h}_2}$. The equations may be simplified a great deal. We regard (10) and (11) as linear equations for $\bar{A}$ and $\bar{P}$. Solving, and using (12) and (13) in (7), we find that the equations that govern the drawing of a capillary are, thus, (in redimensionalized form)

$$\rho\left(h_2^2 - h_1^2\right)\left[u_{0t} + u_0u_{0x} - g\right] = \left[3\mu\left(h_2^2 - h_1^2\right)u_{0x} + \gamma(h_1 + h_2)\right]_x \quad (14)$$
$$\left(h_1^2\right)_t + \left(h_1^2u_0\right)_x = \frac{p_oh_1^2h_2^2 - \gamma h_1h_2(h_1 + h_2)}{\mu\left(h_2^2 - h_1^2\right)} \quad (15)$$
$$\left(h_2^2\right)_t + \left(h_2^2u_0\right)_x = \frac{p_oh_1^2h_2^2 - \gamma h_1h_2(h_1 + h_2)}{\mu\left(h_2^2 - h_1^2\right)} \quad (16)$$

where p_o denotes the dimensional hole overpressure $p_H - p_a$.

In general, (14)–(16) must be solved given initial conditions for $h_1(x), h_2(x)$, and $u_0(x)$, and subject to suitable boundary conditions. For the experimental rig that was used, both h_2 and h_1 were known at the top of the furnace $x = 0$, and the feed speed U_f and the draw speed U_d were prescribed. The boundary conditions are thus

$$h_1(0,t) = h_{10} \qquad h_2(0,t) = h_{20}$$
$$u_0(0,t) = U_f \qquad u_0(L,t) = U_d.$$

It is also worth pointing out that, for the furnace used in the experiments described below, the temperature in the hot zone was assumed to be constant so that the viscosity μ was independent of x.

B. Solutions to the Steady-State Problem

Because we wish to address the manufacturing process for capillaries, for the remainder of this study, we shall be concerned only with time-independent solutions to (14)–(16). If required, the full unsteady versions of the equations may be used to study both startup problems and the stability of the process.

The time-independent versions of (14)–(16) constitute a ordinary differential equation two-point boundary value problem, which must, in general, be solved numerically. To do this, standard library routines may be employed. We implemented the Numerical Algorithms Group, Ltd., (NAG) routine D02HAF, which uses an efficient Runge–Kutta–Merson method (see, for example, [27]).

For the particular capillaries that were drawn experimentally, however, simplifications may be made, because the full generality of (14)–(16) is not required. In particular, progress may be made by examining the orders of magnitude of each term in (14). We find that the inertia and gravity terms on the left-hand side of (14) are unimportant. In addition, the nondimensional ratio $\delta = \gamma L/(\mu h U)$ is small for all $x \le L$ and for all experimental conditions (where h, U and L are defined at the start of Section II-A). Thus, the flow is viscosity-dominated, and we may, therefore, conveniently regard (14)–(16) as a regular perturbation problem in δ. Solving the equations now becomes a simple matter, and we find that

$$u_0 = U_fe^{\beta x/L} + \frac{2\gamma Le^{\beta x/L}}{3\mu\beta(h_{20} - h_{10})} \times \left[e^{-\beta x/2L} - 1 + \left(\frac{x}{L}\right)(1 - e^{-\beta/2})\right] \quad (17)$$
$$h_1 = h_{10}e^{-\beta x/2L} + \frac{\gamma Le^{-\beta x/L}}{3\mu\beta U_f(h_{20} - h_{10})} \times \left[(3h_{20} - h_{10})(1 - e^{\beta x/2L}) + \left(\frac{h_{10}x}{L}\right)e^{\beta x/2L}(e^{-\beta/2} - 1)\right] \quad (18)$$
$$h_2 = h_{20}e^{-\beta x/2L} + \frac{\gamma Le^{-\beta x/L}}{3\mu\beta U_f(h_{20} - h_{10})} \times \left[(3h_{10} - h_{20})(1 - e^{\beta x/2L}) + \left(\frac{h_{20}x}{L}\right)e^{\beta x/2L}(e^{-\beta/2} - 1)\right] \quad (19)$$

where

$$\beta = \ln(U_d/U_f).$$

To leading order, the temperature dependence in this problem, therefore, appears only via the ratio of the surface tension to the viscosity. Equations (17)–(19) can be used to predict the degree of collapse in the final structure, and suggest that this depends only upon the ratio of the surface tension to the viscosity. The perturbation solution (17)–(19) has the advantage that the phenomenological behavior of the solution is readily apparent.

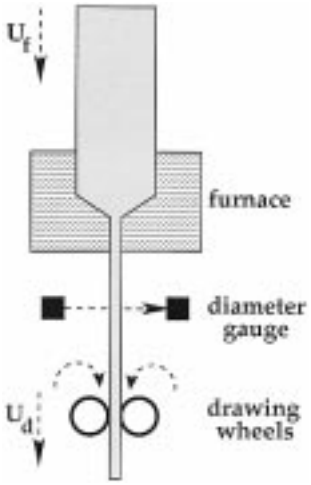

Fig. 3. Schematic diagram of experimental drawing apparatus.

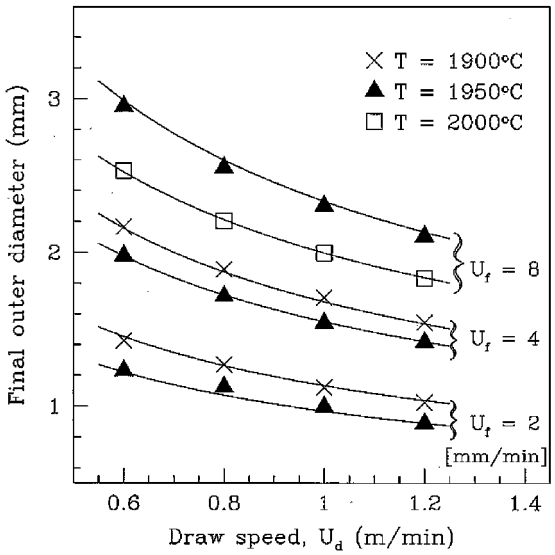

Fig. 4. Experimental results (symbols) and theoretical predictions using (19) for drawn outer capillary diameter as functions of draw speed for a range of furnace temperatures and feed speeds.

However, for more general drawing conditions where the perturbation approximations may not be appropriate, the full boundary value problem must be solved.

III. Experimental Study

In order to check the validity of the model, we performed a simple capillary drawing experiment. This was done using a silica capillary tube with an OD of 28 mm and an inner diameter (ID) of 24 mm as the preform. The glass used was Suprasil F300 (Heraeus Amersil, Inc., Duluth, GA 30096), which is a commercially available high-quality low-impurity grade of silica that is commonly used for the production of low-loss optical fibers.

The preform was heated using a graphite furnace in a conventional commercially available 5-m-high fiber drawing tower (Heathway Limited, Wolverton Mill, Milton Keynes MK12 6LA, U.K.) over a 3-cm hot zone. The preform was fed into the furnace at a constant speed, and the top end of the tube was left open to the atmosphere. A laser-based diameter gauge was located approximately 1 m below the furnace exit, and this was used to monitor the final diameter of the capillary. The draw speed was fixed by passing the drawn capillaries through a pair of wheels whose surface is designed to avoid slippage. A schematic diagram of the drawing arrangement is shown in Fig. 3.

For the purposes of this study, 24 experimental runs were carried out. The feed speed U_f was varied between 2 and 8 mm/min, the draw speed U_d was varied from 0.6 to 1.2 m/min, and furnace temperatures T of 1900, 1950, and 2000 °C were used. Once any particular combination of drawing conditions was set, the process was allowed to stabilize before the final dimensions of the capillary were measured. Owing to the relatively large distance between the drawing wheels and the neck-down region, the system stabilized more quickly at lower temperatures as a result of the rapid increase of viscosity with reduced temperature.

The final OD of each capillary was measured both using the diameter gauge and a micrometer, while the final IDs were extracted from measurements made using an optical microscope. The validity of our ID measurements was also confirmed using the law of mass conservation, which requires that, in steady state, the feed and draw volume fluxes of glass are equal. Our experimental results showed only small deviations from this requirement, with a maximum error in volume flux of just over 5%, although the error was less than 2% for the majority of the experiments. This indicates not only that the final capillary dimensions had been measured accurately, but also that the process had stabilized sufficiently, prior to measurement.

The final measured outer diameters of the drawn capillaries are shown (symbols) as a function of the draw speed U_d for a range of feed speeds and furnace temperatures in Fig. 4. Fig. 5 shows the corresponding final inner diameters. The basic trends are unsurprising; for example, faster draw speeds, higher temperatures, and lower feed speeds all result in reduced capillary inner and outer dimensions.

The theoretical predictions from (19) are indicated by solid lines in Figs. 4 and 5, and were calculated as follows. We set $x = L = 3$ cm in (19) and used the known experimental values for U_f, U_d, h_{10}, and h_{20}. One further piece of information, namely the ratios γ/μ at each furnace operating temperatures, is required. This does not appear to be available for the grade of silica used in these experiments, namely, Suprasil F300. Therefore, for each furnace temperature, we fitted the theoretical model to the experimental data by choosing the parameter γ/μ. The relevant values for 1900, 1950, and 2000°C were 1.606×10^{-6} m/s, 3.847×10^{-6} m/s, and 1.116×10^{-5} m/s, respectively. These values are consistent with the conventional premise that, in this regime, the surface tension is a weak function of temperature but the viscosity decreases exponentially with increasing temperature (see, for example [26]). Although, as noted previously, values for the required viscosity–surface tension ratio do not seem to be available, it is, nevertheless, possible to compare our fitted ratios with published data for vitreous silica found in [28]. From [28, pp. 226 and 641], we find, respectively, that $\mu = 3.7 \times 10^4$ kg/m/s and $\gamma = 0.3$ N/m at a temperature of 2000°C and, thus, $\gamma/\mu \sim 8 \times 10^{-6}$, which is consistent

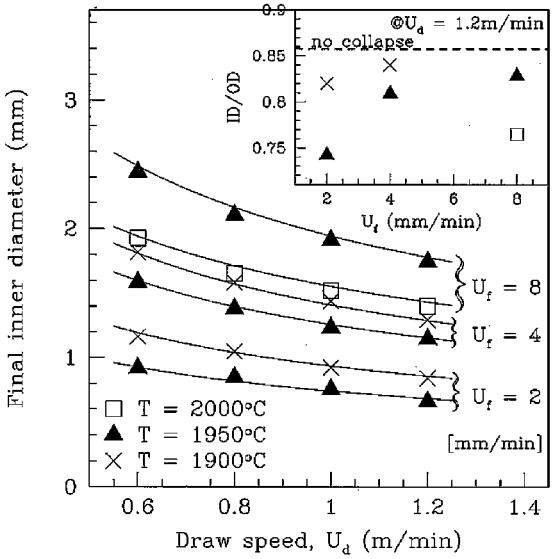

Fig. 5. Experimental results (symbols) and theoretical predictions using (18) for drawn inner capillary diameter as functions of draw speed for a range of furnace temperatures and feed speeds. The inset shows the drawn diameter ratio for draw speed of 1.2 m/min for various furnace temperatures.

with our fitted value. It is also possible to carry out a calculation to determine the activation energy of the viscosity, based on our three data points. Assuming that the surface tension is constant, we find activation energies in the range 129–165 kcal/mol. Given all of the uncertainties involved, this compares favorably with the value of 123 kcal/mol given in [28].

The comparison between the theory and the experimental results is striking, suggesting that the theoretical model is a powerful predictive tool for capillary drawing. Essentially, the 48 experimental points in Figs. 4 and 5 have been theoretically reproduced using only three fitting parameters. It should be noted that the fact that the experimental measurements exhibited only small departures from the requirements of mass conservation means that, effectively, the inner and outer diameters are not truly independent. We conclude that, for a fixed temperature, the theory is particularly good at predicting capillary diameter as a function of both draw and feed speed.

The inset in Fig. 5 shows that the experiments were not geometry-preserving, and some collapse occurred from the original diameter ratio of $24/28 \approx 0.857$. The amount of collapse was relatively small. Although experiments with larger collapse ratios can be performed, they are harder to control and more sensitive to the drawing conditions. This, of course, is one of the prime reasons for developing a theoretical modeling capability, as this provides insight into the sensitivity of the collapse as a function of the control parameters.

IV. Discussion and Manufacturing Implications

In Section III, we have shown that the theoretical predictions for capillary drawing agree well with the experimental results. The theoretical methods developed here may now be used to examine further aspects of the manufacturing process. For example, let us consider how (17)–(19) may be used to predict the degree to which the hole collapses during drawing. We consider the case when $x = O(L)$ and make the approximation $\exp(\beta/2) \gg 1$, which corresponds to the practically relevant case of large draw ratio. Equations (18) and (19) become

$$h_1 = e^{-\beta x/2L}\left[h_{10} + \frac{\gamma L(-3h_{20} + h_{10}(1 - x/L))}{3\mu\beta U_f(h_{20} - h_{10})}\right]$$
$$h_2 = e^{-\beta x/2L}\left[h_{20} + \frac{\gamma L(-3h_{10} + h_{20}(1 - x/L))}{3\mu\beta U_f(h_{20} - h_{10})}\right]$$

and, defining the collapse ratio C by

$$C = 1 - \frac{h_1 h_{20}}{h_{10} h_2}$$

so that total collapse occurs when $C = 1$ but the preform geometry is faithfully preserved when $C = 0$, we find, on using the fact that $\delta \ll 1$, that many simplifications occur and

$$C = \frac{\gamma L}{\mu U_f \ln(U_d/U_f)}\left[\frac{h_{10} + h_{20}}{h_{10} h_{20}}\right]. \tag{20}$$

This expression allows us to interpret the sensitivity of the collapse to the physical parameters in the problem. We note, first, that (20) is independent of x/L to leading order. This indicates that any collapse that does occur does so when $x = O(L/\beta)$, i.e., in the upper part of the furnace. Over the remaining larger part of the furnace, although the fiber diameter reduces, the fiber geometry is nearly constant. This may seem counterintuitive because the surface tension forces that cause the collapse increase as the radius of the capillary decreases. Although this is indeed so, the applied tension induced by the drawing process causes the viscous forces to increase more rapidly with decreasing capillary size, so that the influence of surface tension is most significant where the capillary has the largest diameter.

Other manufacturing conclusions may also be drawn from (20). In particular, C depends on the draw and feed speeds only through the quantity $(U_f \ln(U_d/U_f))^{-1}$, and, hence, is much more sensitive to feed speed than draw speed. As far as the geometry is concerned, C depends only upon the quantity

$$\frac{1}{h_{10}}\left(1 + \frac{h_{10}}{h_{20}}\right)$$

and is, therefore, much more sensitive to the preform inner diameter h_{10} than to its initial wall thickness ratio as characterized by h_{10}/h_{20}, which can lie only in the range $0 \le h_{10}/h_{20} \le 1$. The hot-zone length L is dictated by the furnace design, and (20) shows that the collapse depends linearly upon L. The collapse is, therefore, relatively insensitive to the hot-zone length. The collapse also depends upon the furnace temperature, which manifests itself via the ratio γ/μ in (20). Our results above indicate that for Suprasil F300, a temperature change of 100°C results in γ/μ changing by a factor of about 10; this behavior can be taken to be typical for similar silica materials. We conclude that relatively modest temperature changes of around 10°C may materially affect the collapse ratio.

It is tempting to use (18) to predict when pinch-off will occur and the hole in the drawn fiber will vanish completely. Still assuming that $\exp\beta/2 \gg 1$, we find that the condition for

pinch-off to occur at some position before $x = L$ (i.e., in the furnace) becomes

$$\mu h_{10}(h_{20} - h_{10})U_f \ln(U_d/U_f) < \gamma L h_{20}. \qquad (21)$$

Although (21) is not strictly valid, owing to the nonuniformity of the small δ expansion in this limiting case, in many circumstances, it may be expected to give practical insight into when pinch-off occurs.

Another fabrication regime of practical interest concerns the manufacture of fibers in which the preform geometry is preserved. In such cases, the quantity C in (20) should be small and the asymptotic approximations are, consequently, particularly accurate. This may be accomplished by using a short hot zone, a low temperature, a high feed speed, a large inner diameter, or any combination of these.

V. Conclusion

An asymptotic fluid mechanics model has been posed for the drawing of capillaries. The theory not only gives good agreement with experiment, but suggests a number of both qualitative and quantitative conclusions about the process of capillary drawing that are practically relevant to holey fiber manufacture.

Space does not permit a full discussion of a number of ways in which the model may easily be refined. In any case, (14)–(16) are relevant not only for capillary manufacture but also for a wide range of other practical circumstances. In other regimes (for example, pressurized holes), different terms in the governing equations become important and different asymptotic limits may be analyzed. The model is also readily applicable to drawing processes involving other materials such as compound glasses (see, for example [29]).

At present, the theory applies only to the case where one symmetrically placed circular hole is present. The analysis may readily be extended to investigate the stability of symmetric capillary drawing, as well as to investigate the effect of any slight asymmetries that may be present in the initial preform.

For geometries in which multiple holes are present, as in a holey fiber, the lack of circular symmetry renders the analysis more complicated. In such cases, the general methodology first set out in [30] may be employed. The details of the application of this approach to practical structures will be explained in a future study.

Acknowledgment

The authors wish to thank D. Richardson, N. Broderick, and A. Wheeler for useful discussions.

References

[1] T. A. Birks, J. C. Knight, and P. St. J. Russell, "Endlessly single-mode photonic crystal fiber," *Opt. Lett.*, vol. 22, pp. 961–963, 1997.

[2] T. M. Monro, D. J. Richardson, and P. J. Bennett, "Developing holey fibers for evanescent field devices," *Electron. Lett.*, vol. 35, pp. 1188–1189, 1999.

[3] T. M. Monro, D. J. Richardson, N. G. R. Broderick, and P. J. Bennett, "Holey optical fibers: An efficient modal model," *J. Lightwave Technol.*, vol. 17, pp. 1093–1102, June 1999.

[4] J. K. Ranka, R. S. Windeler, and A. J. Stentz, "Optical properties of high-delta air-silica microstructure optical fibers," *Opt. Lett.*, vol. 25, pp. 796–798, 2000.

[5] J. C. Knight, T. A. Birks, R. F. Cregan, P. St. J. Russell, and J. P. de Sandro, "Large mode area photonic crystal fiber," *Electron. Lett.*, vol. 34, pp. 1347–1348, June 25, 1998.

[6] T. A. Birks, D. Mogilevtsev, J. C. Knight, and P. S. Russell, "Dispersion compensation using single-material fibers," *IEEE Photon. Technol. Lett.*, vol. 11, pp. 674–676, June 1999.

[7] T. M. Monro, D. J. Richardson, and N. G. R. Broderick, "Efficient modeling of holey fibers," presented at the OFC'99, San Diego, CA, Feb. 21–26, 1999. Paper FG3.

[8] A. Ferrando, E. Silvestre, J. J. Miret, and P. Andres, "Nearly zero ultraflattened dispersion in photonic crystal fibers," *Opt. Lett.*, vol. 25, pp. 790–792, 2000.

[9] J. C. Knight, J. Broeng, T. A. Birks, and P. St. J. Russell, "Photonic band gap guidance in optical fibers," *Science*, vol. 282, pp. 1476–1478, 1998.

[10] M. Key, I. G. Hughes, W. Rooijakkers, B. E. Sauer, E. A. Hinds, D. J. Richardson, and P. G. Kazansky, "Propagation of cold atoms along a miniature magnetic guide," *Phys. Rev. Lett.*, vol. 84, pp. 1371–1373, 2000.

[11] M. A. Matovich and J. R. A. Pearson, "Spinning a molten threadline—Steady-state isothermal viscous flows," *Ind. Eng. Chem. Fund.*, vol. 8, pp. 512–520, 1969.

[12] J. R. A. Pearson and M. A. Matovich, "Spinning a molten threadline—Stability," *Ind. Eng. Chem. Fund.*, vol. 8, pp. 605–609, 1969.

[13] Y. T. Shah and J. R. A. Pearson, "On the stability of nonisothermal fiber spinning," *Ind. Eng. Chem. Fund.*, vol. 11, pp. 145–149, 1972.

[14] ——, "On the stability of nonisothermal fiber spinning—General case," *Ind. Eng. Chem. Fund.*, vol. 11, pp. 150–153, 1972.

[15] F. T. Geyling and G. M. Homsy, "Extensional instabilities of the glass fiber drawing process," *Glass Technol.*, vol. 21, pp. 95–102, 1980.

[16] F. T. Geyling, "Basic fluid dynamic considerations in the drawing of optical fibers," *Bell Syst. Tech. J.*, vol. 55, pp. 1011–1056, 1976.

[17] J. N. Dewynne, P. D. Howell, and P. Wilmott, "Slender viscous fibers with inertia and gravity," *Q. J. Mech. Appl. Math.*, vol. 47, pp. 541–555, 1994.

[18] J. Dewynne, J. R. Ockendon, and P. Wilmott, "On a mathematical-model for fiber tapering," *SIAM J. Appl. Math.*, vol. 49, pp. 983–990, 1989.

[19] H. Papamichael and I. N. Miaoulis, "Thermal-behavior of optical fibers during the cooling stage of the drawing process," *J. Mater. Res.*, vol. 6, pp. 159–167, 1991.

[20] S. E. Rosenberg, H. Papamichael, and I. N. Miaoulis, "A 2-dimensional analysis of the viscous problem of a glass preform during the optical-fiber drawing process," *Glass Technol.*, vol. 35, pp. 260–264, 1994.

[21] Z. L. Yin and Y. Jaluria, "Thermal transport and flow in high-speed optical fiber drawing," *J. Heat Transfer Trans. ASME*, vol. 120, pp. 916–930, 1998.

[22] P. Gospodinov and A. L. Yarin, "Draw resonance of optical microcapillaries in nonisothermal drawing," *Int. J. Multiphase Flow*, vol. 23, pp. 967–976, 1997.

[23] A. L. Yarin, P. Gospodinov, and V. I. Roussinov, "Stability loss and sensitivity in hollow fiber drawing," *Phys. Fluids*, vol. 6, pp. 1454–1463, 1994.

[24] S. D. Sarboh, S. A. Milinkovic, and D. L. J. Debeljkovic, "Mathematical model of the glass capillary tube drawing process," *Glass Technol.*, vol. 39, pp. 53–67, 1998.

[25] M. Hucker, I. Bond, A. Foreman, and J. Hudd, "Optimization of hollow glass fibers and their composites," *Adv. Comp. Lett.*, vol. 8, pp. 181–189, 1999.

[26] S. H.-K. Lee and Y. Jaluria, "Simulation of the transport processes in the neck-down region of a furnace drawn optical fiber," *Int. J. Heat Mass Transfer*, vol. 40, pp. 843–856, 1997.

[27] G. Hall and J. M. Watt, Eds., *Numerical Methods for Ordinary Differential Equations*. Oxford, U.K.: Clarendon, 1976.

[28] N. P. Bansal and R. H. Doremus, *Handbook of Glass Properties*. New York: Academic, 1986.

[29] T. M. Monro, Y. D. West, D. W. Hewak, N. G. R. Broderick, and D. J. Richardson, "Chalcogenide holey fibers," *Electron. Lett.*, vol. 36, pp. 1998–2000, 2000.

[30] P. D. Howell, "Extensional Thin Layer Flows," Ph.D. dissertation, Oxford Univ., Oxford, U.K., 1994.

Alistair D. Fitt received the D.Phil. degree from Oxford University, Oxford, U.K., in 1983 for his work on the film cooling of turbine blades.

He carried out defense-related research at Royal Military College of Science, Shrivenham, Swindon, U.K., for five years before joining the Mathematics Department at the University of Southampton, Southampton, U.K., in 1989. He has worked on a wide range of industrially oriented applied mathematics problems and has been a frequent contributor to the European Study Groups with Industry meetings.

Kentaro Furusawa was born in Tokyo, Japan. He received the B.Sc. and M.Sc. degrees from Keio University, Tokyo, Japan, in 1998 and 2000, respectively. He is now pursuing the Ph.D. degree at the Optoelectronics Research Centre, University of Southampton, Southampton, U.K., in the fabrication and characterization of microstructured fibers.

Tanya M. Monro received the Ph.D. degree from Sydney University, Sydney, Australia.

She holds a Royal Society University Research Fellowship at the Optoelectronics Research Centre (ORC), University of Southampton, Southampton, U.K. She joined the ORC in 1998, and works on designing and developing novel waveguides including holey optical fibers and self-written waveguides.

Dr. Monro received the Bragg Gold Medal for the best physics Ph.D. dissertation in Australia in 1998.

Colin P. Please is a Professor in the Mathematics Department, University of Southampton, Southampton, U.K., where he has worked since 1985. His interests are mainly in problem-driven applications of mathematics including those with diffusion and fluid flow aspects. He currently studies problems connected with tumor growth, superconductivity, and liquid crystal devices.